



Photocatalytic activity of $\text{TiO}_2\text{-P25@n-TiO}_2\text{@HAP}$ composite films for air depollution

Guy Didier Fanou, Mamadou Traore, Benjamin Kouassi Yao, Andrei Kanaev, Khay Chhor

► To cite this version:

Guy Didier Fanou, Mamadou Traore, Benjamin Kouassi Yao, Andrei Kanaev, Khay Chhor. Photocatalytic activity of $\text{TiO}_2\text{-P25@n-TiO}_2\text{@HAP}$ composite films for air depollution. *Environmental Science and Pollution Research*, 2021, 28 (17), pp.21326-21333. 10.1007/s11356-020-11924-4 . hal-03412180

HAL Id: hal-03412180

<https://hal.science/hal-03412180>

Submitted on 5 Nov 2021

HAL is a multi-disciplinary open access archive for the deposit and dissemination of scientific research documents, whether they are published or not. The documents may come from teaching and research institutions in France or abroad, or from public or private research centers.

L'archive ouverte pluridisciplinaire **HAL**, est destinée au dépôt et à la diffusion de documents scientifiques de niveau recherche, publiés ou non, émanant des établissements d'enseignement et de recherche français ou étrangers, des laboratoires publics ou privés.

Photocatalytic activity of $\text{TiO}_2\text{-P}_{25}\text{@ n-TiO}_2\text{@HAP}$ Composite Films for Air depollution

Guy Didier FANOU^{1,2}, Mamadou TRAORE¹, Benjamin Kouassi YAO², Andrei KANAIEV¹,
Khay CHHOR¹

¹ *Laboratoire des Sciences des Procédés et des Matériaux, CNRS, Université Paris 13,
Sorbonne Paris Cité, 93430 Villetaneuse, France*

² *Laboratoire des Procédés de Synthèse, de l'environnement et des Energies Nouvelles-
LAPISEN, INPHB ; Côte d'Ivoire*

Corresponding author : traore@lspm.cnrs.fr/ 0149404052 / 0149403414

Abstract

We report on an elaboration of new composite photocatalysts ($\text{TiO}_2\text{-P}_{25}\text{@ n-TiO}_2\text{@HAP}$) based of grafted size-selected 5nm titanium-oxo-alkoxo nanoparticles on $\text{P}_{25}\text{-TiO}_2$ nanoparticles and HAP obtained by co-precipitation of salts. The 5-nm oxo- TiO_2 particles were prepared in a sol-gel reactor with rapid reagents micromixing. The photocatalytic test of ethylene degradation, in a continuous-flow fixed bed reactor, showed an increase of the photocatalytic yield for the composite photocatalysts with an addition of HAP. This result was interpreted by a synergy between adsorption and photooxidation.

Keywords: TiO_2 , hydroxyapatite, composite nanoparticles, photocatalysis.

1.Introduction

The industrial, domestic and military activities are increasingly rejecting toxic materials, especially in recent decades (Jacobson 2002; Atkinson 2000; Jia 2013; Bryne et al. 1998; Guo et al. 2003). The water and air quality is decreasing which represents a serious threat for all living species. Among the possible techniques for the destruction of pollution traces are the

Advanced Oxidation Technologies (TOA), the most important of which are ozonation, the use of ultraviolet (UV), plasma degradation and photocatalysis. From 2000 to 2018, the number of publications on TOA increases by more than fourfold and reaches 7000 publications (Giwa et al, 2021). Honda and Fujishima (1972) suggested the use of TiO_2 excited by ultraviolet radiation to decompose organic pollutants.. The principle of photocatalysis involves photogeneration of electron-hole pairs. Under light excitation, the electrons (e^-) of the valence band (BV) of the TiO_2 pass to the conduction band (BC), leaving a positive charge or hole (noted h^+) in the BV. These electron-hole pairs can recombine by releasing heat, or react separately with pollutant molecules of the environment. The recombination of the photoinduced charges served to be the main shortcoming of the photocatalytic process, which can be reduced by doping of the active component and/or its integration in a composite medium. In this connection, the combination of nano- TiO_2 and HAP may be an interesting solution.

Because of a large band gap energy ~ 7.7 eV ($\lambda = 160$ nm), measured e.g. by Feldbach et al. (2015) and calculated by Tsukada et al. (2011), appreciable photocatalytic activity of this material cannot be expected. However, HAP was capable forming oxygen defects under UV illumination serving as active centers (Nishikawa et al. 2002) and some photocatalytic activity of HAP has been observed on the reduction of methyl mercaptan and dimethyl sulfide (Tanaka et al. 2012). The use of hydroxyapatite (HAP) as an adsorbent material is of increasing interest because of its remarkable property of ion exchange, bonding with organic molecules, low solubility in water (Iliev et al. 2007; Krestou et al. 2004; Ma et al. 1994; Qian et al 2014; Bahdod et al. 2009). Hydroxyapatite also has catalytic properties that have been studied in several fields (Monma 1982; Matsumura et al. 1984; Joris et al. 1971; Kibby et al. 1972; Bett et al., 1968; Matsumura et al. 1994; Matsumura et al. 1997; Chlala 2016): dehydrogenation, dehydration, combustion, oxidation, reforming, etc. Several studies have

focused on the use of the adsorption-photocatalytic coupling of the TiO_2 / HAP composite for the removal of gaseous pollutants (Azouani et al. 2010a; Azouani et al. 2010b; Azouani et al. 2007; Benmami et al. 2006). Thus, NO adsorption was observed by Nonami et al. (2004), Mitsionis et al. (2011) as well as Nasr-Esfahani et al. (2012) in photocatalytic studies. However, the improvement of the gas phase photocatalytic activity due to the presence of hydroxyapatite on the surface of TiO_2 is controversial; a negative or no effect can be observed with regard to the process procedure and the UV wavelengths used. The coupling between TiO_2 and HAP and the overall process efficiency are expected to depend on the process procedure. In this work, we applied a new approach to the photocatalyst synthesis by using titanium oxo-alkoxy (TOA) nanoparticles as a link between TiO_2 P25 and HAP components. The photocatalytic activity of the prepared $\text{TiO}_2\text{-P}_{25}@ \text{n-TiO}_2$ materials has been evaluated.

2. Material and Methods

2.1 Elaboration of $\text{TiO}_2\text{-P}_{25}@ \text{n-TiO}_2$

The general approach to synthesize the $\text{TiO}_2\text{-P}_{25}@ \text{n-TiO}_2$ has been proposed by Fanou et al. (2016). The sol nanoparticles are prepared in the sol–gel reactor using titanium tetraisopropoxide (TTIP) as a precursor. Two stock solutions: 50 cm^3 of a TTIP/propan-2-ol solution and 50 cm^3 of a H_2O /propan-2-ol solution, was synchronously injected under nitrogen into the turbulent mixing zone ($\text{Re} = 4500$) of sol–gel reactor (Azouani et al. 2010b) where the oxo- TiO_2 nanoparticles were generated from hydrolysis condensation reactions. The particle size can be tuned by adjusting the hydrolysis ratio $H = C_{\text{H}_2\text{O}}/C_{\text{TTIP}}$, where $C_{\text{H}_2\text{O}}$ and C_{TTIP} are respectively water and titanium precursor concentrations. We have prepared colloids using hydrolysis ratio $H = 2$, which corresponds to one of stability domains of the sol–gel process and enables particles size of 5.2 nm (Azouani et al. 2007). The suspended

oxoparticles solution was subsequently transferred to a glove box LABstar MBraun where they were combined slowly with TiO₂-P25 powder under stirring. The ratio 66 % of TiO₂-P25/ n-TiO₂ was the same for all prepared samples. A stable nanocoating, with a specific area of 72 m²/g, was prepared by immobilization of nanoparticles on glass bed by dip-coating.

2.2 Elaboration of TiO₂-P₂₅@ n-TiO₂@HAP

Two types of composites were prepared by i) crystallization on the surface of the TiO₂-P25 @ n-TiO₂ of hydroxyapatite in a physiological solution SBF (CPS / HAP-SBF) ii) incorporation of hydroxyapatite in the matrix TiO₂-P25 @ n-TiO₂ (CPS / HAP).

2.2.1 Co-precipitation method

The chemicals (Sigma Aldrich) involved in this experiment are calcium nitrate Ca(NO₃)₂·4H₂O (purity 99%), ammonium dihydrogen phosphate NH₄H₂PO₄ (purity ≥ 98%) and Ammonia (purity 99,5%). 125 ml of calcium nitrate (0.5 mol.L⁻¹) and 75 ml of ammonium phosphate (0.5 mol.L⁻¹) are mixed with vigorous stirring. Then, concentrated ammonia is added dropwise to pH≈10-10.5 to give a white precursor precipitate of HAP. After stirring for 1 hour, the suspension is filtered and stored in a hermetically sealed beaker in order to avoid carbonation due to atmospheric carbon dioxide. HAP is then mixed with the colloid suspension TiO₂-P₂₅@n-TiO₂ so as to obtain different mass percentage. The mixture of the hydroxyapatite and composite particles are immobilized by dip-coating on the 1 mm diameter glass beads for photocatalytic tests. Prepared materials are noted as CPS / HAP.

2.2.2 Simulated Body Fluid (SBF) method

This preparation method is advocated by Li et al. (1993). The chemicals were purchased from Sigma Aldrich in quantities indicated in Table 1.

In general, 250 ml of distilled water were poured into a beaker and placed in a water bath at 36.5 °C with magnetic stirring. Each reagent was then subsequently added to the reaction medium during the synthesis. The pH was adjusted to 7.25 using 1N HCl. At the end, the volume of the solution was completed to 500 mL with distilled water and stored in a refrigerator at 5-10 °C. The crystallization of hydroxyapatite on TiO₂-P25 @ n-TiO₂ composite was carried out by placing the composite samples and the SBF solution in contact under slight agitation. The crystallization time varies from 30 min to 5h. Longer calcination times were also used in the preparation and specified if applicable. Prepared materials are noted as CPS / HAP-SBF.

2.3. Photocatalyst Characterization

The prepared samples were structurally characterised by X-ray diffraction XRD (INEL XRG 3000) using CuK α radiation with Nickel filter. The surface morphology of photocatalyst was examined by SEM JEOL JSM 64400F with acceleration voltage of 10 kV. Raman spectra were measured at 516 nm using micro-Raman high-resolution HR800 installation (HORIBA JobinYvon) with the spectral and spatial resolution respectively 0.25 cm⁻¹ and 5 μ m. The scattered light is collected by Peltier cooled CCD camera in a backscattering configuration. The photocatalytic activity of the prepared samples was tested in a continuous-flow fixed-bed reactor on ethylene decomposition. A gas flow of pollutant (120 ppm) mixture with dry air and flow rate of 7.5 mL/min passes through a reactor tube of 6-mm diameter and 35 cm length made of glass transparent in the UV-A spectral range (Benmami et al. 2005; Tieng et al. 2011). The glass beads coated photocatalyst samples were filled the reactor tube of 15 cm length around the middle. Inside the tube, just after the glass bead, a chromel / alumel thermocouple monitors the temperature. The tube is surrounded at a radial distance of 3 cm by six 8-W lamps of 29 cm length emitting at 362 nm ($\Delta\lambda_{\text{hwm}} = 22$ nm). During the experiments,

the reactor is cooled by compressed air stream. Ethylene concentrations before (C_{in}) and after (C_{out}) the photocatalytic reactor were monitored by online gas chromatography (Varian 191 CP 3800) equipped with a capillary column (HP-PLOT/Q) and a flame ionization detector FID. Before turn on the UV lamps, one hour period is applied for the stabilization of Ethylene concentrations and the gas inlet stream temperature at 25 °C. Two injection loops of 250 µL and heated at 80 °C allow measurements of pollutant concentration in continuous mode. The reactor yield (or ethylene conversion) is calculated according to the formula: $\eta(\%) = (C_{in} - C_{out})/C_{in} \times 100$. The column temperature and flow rate of the carrier gas (N_2) were respectively 50 °C and 5 mL/min.

3. Characterization

3-1. X-ray diffraction

The X-ray plots of pure hydroxyapatite (figure 1) show well-defined peaks indicating that the solids are well crystallized.

In the range of 2θ between 25 and 35 °, they reveal clear diffractions of the (002) planes at 25.7 ° and those of the (211), (300), and (202) planes at 31.6, 32, 7 ° and 33.9 ° respectively. All these planes can be indexed in the hexagonal space group system P63 / m (Nathanael et al. 2010). The average size of the crystallites was estimated using the Sherrer formula (Smith 1989) and the Bragg reflection of the (002) planes. These parallel planes with the c^{\rightarrow} axis represent the preferential direction of growth of the hydroxyapatite.

$$d = \frac{k\lambda}{b(2\theta) \cos \theta}$$

d is the diameter of the crystallites (Å), k is a constant (0.9), λ is the incident wavelength (Å), θ is the Bragg angle (degree) and b is the half width. recorded peak height expressed in radians.

The calculated value of d is close to 21 nm for the sample treated at 100 ° C. and 22.5 nm for that calcined at 450 ° C.

The X-ray diffraction patterns of the samples of the TiO₂-P25 @ n-TiO₂ composite containing a dispersion of HAPs are shown in Figure 2.

The spectra show a presence of crystallized HAP in the material. The intensity of the most intense HAP peaks around 31.5 ° increases with the increase in its mass content in the material. They appear clearly in the sample diagram with 30% PAH.

3-2. Raman spectroscopy

The vibrational study by Raman scattering was recorded on the powders of the following samples:

i) Pure hydroxyapatite treated at 450 ° C.

ii) TiO₂-P25 @ n-TiO₂ / PAH noted CPS / HA with a mass content equal to 3 and 5% of incorporated PAH.

The spectrum of hydroxyapatite is shown in Figure 3.

The frequency range between 400 and 1200 cm⁻¹ characterizes the diffusion bands of the (PO₄)³⁻ group. The peaks observed around 430 and 449 cm⁻¹ can be attributed to the deformation vibration ν_2 . The Raman bands at 580, 592 and 610 cm⁻¹ correspond to the triple degenerate vibrational mode ν_4 . The symmetrical elongation vibration mode ν_1 of the (PO₄)³⁻ group appears as a very intense peak located at 962 cm⁻¹. This diffusion band is characteristic of the structure of hydroxyapatite (Smeulders, 2001). The antisymmetric vibration ν_3 can be associated with the diffusion bands observed at 1032, 1048 and 1079 cm⁻¹. Figure 4 shows the

Raman spectra of the TiO₂-P25 @ n-TiO₂ / HAP (CPS / HAP) composite with a mass content of 3 and 5% PAH.

The spectra obtained clearly show three Raman bands at 399, 516 and 642 cm⁻¹ of the anatase of the composite. As for the hydroxyapatite, because of its low concentration in the matrix (3 and 5%) the intensity of the diffusion bands is very weak making the observation difficult. The only detectable peak is 962 cm⁻¹ attributed to the vibrational mode ν_1 of the (PO₄)³⁻ group.

4. Photocatalytic activity

4-1. Co-precipitation method

The photocatalytic tests were measured on the samples of 0.5% and 1% by weight of hydroxyapatite with the references CPS / HAP-0.5 and CPS / HAP-1 respectively. Figure 5 shows the evolution of photocatalytic activity of ethylene degradation.

The conversion of ethylene to CPS / HAP-0.5, CPS / HAP-1 shows a rapid increase for 20 min under UV radiation. As Tieng et al have already observed (2011), the warm up time of UV lamps was too short (Figure 6a) to account for this behavior. The temperature increases from 25 °C to 46 ± 2 °C in about 3 min. Moreover no photolysis of ethylene is observed (Figure 6b). The delay in the achievement of the asymptotic ethylene conversion has been previously explained by the formation of non-volatile intermediate reaction products, assigned to the oxidized polymeric hydrocarbons: furan and furfural oligomers Ol_N with N=6÷8 (Tieng et al. 2019). After this step, the photocatalytic yield reaches a stable steady state corresponding to a conversion value η greater than that of the reference composite: 12% for CPS / HAP-1 and

6% for CPS / HAP-0.5. The first order rates of the pollutant decomposition in Figure 7, which reflects the intrinsic photocatalyst activity (Fanou et al. 2016), showed a linear proportionality to the HAP content. It begins however from a non-zero value, characteristic of the pure titania activity, increasing by ~50% at 1wt% of HAP.

This enhancement might be associated with: i) strong adsorption capacity of hydroxyapatite with respect to the pollutant and the secondary reaction products likely to form during the photocatalytic reactions (Hauchecorne et al. 2011), ii) better availability of active sites because of elimination of poisons by adsorbance on the composite surface, and iii) charge separation efficiency enhancement in the composite. Mitsionis et al. (2011) have reported that the formation of OH^\bullet radicals is greater onto HAP / TiO_2 composite than TiO_2 alone. In the same time, the band gap energy of HAP/ TiO_2 composite $E_g=3.08$ eV (Kamat 2002) has been reported to be insignificantly lower compared with pure titania (3.12 eV), whereas that of HAP reported by Feldbach et al. (2015) and Lopez et al. (2013) was significantly larger: 7.7 eV and >6 eV respectively. Accordingly, synergistic effect between adsorbing and active sites could be responsible for the enhanced activity of the composite. The following scenario highlighting the synergistic action of these two components, composite and adsorbent, can be described as follows: the molecules of the pollutant are additionally adsorbed by HAP and then migrate along the composite surface to the active nanoparticles where they react. The secondary products, if formed, can be advantageously captured by HAP discharging active sites to be decomposed on a later stage.

4-2. SBF method

Figure 8 shows the results of the photocatalytic activity of the films prepared with a crystallization time of 30 min.

The obtained results indicate that the ethylene conversion η increases rapidly for about 20 minutes of irradiation to reach a maximum of 3% to 5% higher than that of the reference ($\text{TiO}_2\text{-P25 @ n-TiO}_2$). We also explained this behavior by the thermal activation of the material following the rise of temperature. It then shows a slow decrease to a lower value than that of the untreated sample after about 40 minutes. This behavior is fairly reproducible for the three samples. Different reasons can explain this behavior : (i) scattering of the incident light by the surface particles (ii) e^-/h^+ charge transfer blocking at the composite-hydroxyapatite interface of the composite to the adsorbed ethylene (Feldbach et al. 2015; Tsukada et al. 2011), iii) poisoning of sites material assets by the presence of products from the elaboration stage.

In order to confirm these hypotheses, we studied the influence of the crystallization time on the photocatalytic activity shown in Figure 9. The results show the similar behavior observed on Figure 8 and the maximum ethylene conversion is also obtained at the same time (30-40 min).

We observe that the prolonged crystallization time decreases the photocatalytic activity of the composite material. This reduction in photocatalytic performance is important and varies from 5% (30 min) to 75% for a crystallization time of 5 h. These results support the explanations we have advanced above: hydroxyapatite on the surface, increase the scattering of the incident light and reduce the charges transfer at the interface and the crystallization products can poison the photocatalyst.

The different performances of the two prepared $\text{TiO}_2\text{-P}_{25}\text{@ n-TiO}_2\text{@HAP}$ materials (Figures 5 and 8) can be explained by their probable structure. Hydroxyapatite crystals deposited on the surface of $\text{TiO}_2\text{-P}_{25}\text{@ n-TiO}_2$ is obtained by the SBF method. In this case, an increase of crystallization time causes a decrease of the photocatalytic activity. Whereas,

when hydroxyapatite crystals are incorporated in the $\text{TiO}_2\text{-P}_{25}\text{@ n-TiO}_2$ matrix, it is dispersed in the composite and can create a synergistic effect of hydroxyapatite on the photooxidation properties of the photocatalyst.

4. Conclusion

Two families of new composite photocatalysts were prepared by crystallization on the surface of the $\text{TiO}_2\text{-P}_{25}\text{@ n-TiO}_2$ of the hydroxyapatite in a physiological solution SBF and by incorporation of hydroxyapatite in $\text{TiO}_2\text{-P}_{25}\text{@ n-TiO}_2$ matrix. Both HAP and TiO_2 conserve own crystallinity in the material. The photocatalytic yield (gas phase conversion of ethylene) of the material obtained by co-precipitation was increased with an increase of the HAP content, indicating the synergy between two components. On the other hand, the prolonged crystallization time of the composite in SBF has a negative effect on the photocatalytic yield.

275 **Declarations**

276 Ethics approval and consent to participate :

277 Not applicable

278 Consent for publication :

279 Not applicable

280 Availability of data and materials :

281 The datasets used and/or analysed during the current study are available from the
282 corresponding author on reasonable request.

283 Competing interests :

284 The authors declare that they have no competing interests

285 Funding :

286 Not applicable

287 Authors' contributions :

288 All authors (Guy Didier FANOU, Mamadou TRAORE, Benjamin Kouassi YAO, Andrei
289 KANAIEV and Khay CHHOR) contributed to the study conception and design. Material
290 preparation, data collection and analysis were performed by Guy Didier FANOU. The first
291 draft of the manuscript was written by Mamadou TRAORE and other authors (Guy Didier
292 FANOU, Benjamin Kouassi YAO, Andrei KANAIEV and Khay CHHOR) commented on
293 previous versions of the manuscript. All authors (Guy Didier FANOU, Mamadou TRAORE,
294 Benjamin Kouassi YAO, Andrei KANAIEV and Khay CHHOR) read and approved the final
295 manuscript.

296 Acknowledgements :

297 Not applicable

References

- Atkinson R. (2000), Atmospheric chemistry of VOCs and NO_x, Atmos. Environ. 34 : 2063–2101.
- Azouani R., Michau A., Hassouni K., Chhor K., Bocquet J.-F., Vignes J.-L., Kanaev A. (2010), Elaboration of pure and doped TiO₂ nanoparticles in sol–gel reactor with turbulent micromixing: Application to nanocoatings and photocatalysis, Chem. Eng. Res. Des. 88 : 1123–1130.
- Azouani R., Soloviev A., Benmami M., Chhor K., Bocquet J.-F., Kanaev A. (2007), Stability and growth of titanium-oxo-alkoxy Ti_xO_y(OiPr)_z clusters, J. Phys. Chem. C. 111 : 16243–16248.
- Azouani R., Tieng S., Chhor K., Bocquet J.-F., Eloy P., Gaigneaux E. M., Klementiev K., Kanaev A. (2010), TiO₂ doping by hydroxyurea at the nucleation stage: towards a new photocatalyst in the visible spectral range, Phys. Chem. Chem. Phys. 12 : 11325–11334.
- Bahdod A., El Asri S., Saoiabi A., Coradin T., Laghzizil A. (2009), Adsorption of phenol from an aqueous solution by selected apatite adsorbents: Kinetic process and impact of the surface properties, Water Res. 43 : 313–318.
- Benmami M., Chhor K. and Kanaev A. (2005) Supported nanometric titanium oxide sols as a new efficient photocatalyst, J Phys Chem B, 109: 19766- 19771.
- Benmami M., Chhor K. and Kanaev A. (2006), High photocatalytic activity of monolayer nanocoatings prepared from non-crystalline titanium oxide sol nanoparticles, Chem. Phys. 442 : 552–557.
- Bett J.A., Hall W.K. (1968), The microcatalytic technique applied to a zero order reaction: The dehydration of 2-butanol over hydroxyapatite catalysts, J. Catal. 10 : 105–113.

321 -Byrne J.A., Eggins B. R., Brown N.M.D., McKinney B., Rouse M. (1998), Immobilisation
 322 of TiO₂ powder for the treatment of polluted water, *Appl. Catal. B Environ.* 17 : 25–36.

323 -Chlala D., Labaki M., Giraudon J., Lamonier J. (2016), Toluene total oxidation over Pd and
 324 Au nanoparticles supported on hydroxyapatite, *Comptes Rendus Chimie*, 19 : 525-537.

325 -Fanou G.D., Yao B., Cheng K., Brinza O., Traore M., Kanaev A., Chhor K. (2016),
 326 “Elaboration of novel nanoparticulate TiO₂-P25@nTiO₂ composite for Catalysis”,
 327 *International Journal of Advanced Applied Physics Research* 3 : 19-25.

328 -Feldbach E., Kirm M., Kotlov A., Mägi H. (2015), Luminescence Spectroscopy of Ca-
 329 apatites under VUV Excitation, *User Rep. Mater. Sci. Http photon-Sci. Desy* . 17 : 122–123.

330 -Fujishima A., Honda K. (1972), TiO₂ photoelectrochemistry and photocatalysis, *Nature*. 238
 331 : 37–38.

332 -Giwa A., Yusuf A., Balogun H. A, Sambudi N. S., Bilad M. R., Adeyemi I., Chakraborty S.
 333 Curcio S. (2021), Recent advances in advanced oxidation processes for removal of
 334 contaminants from water: A comprehensive review, *Process Safety and Environmental*
 335 *Protection*, 146 : 220-256

336 -Guo F.Q., Okamoto M., Crawford N. M. (2003), Identification of a plant nitric oxide
 337 synthase gene involved in hormonal signaling, *Science*. 302 : 100–103.

338 -Hauchecorne B., Tytgat T., Verbruggen S.W., Hauchecorne D., Terrens D., Smits M.,
 339 Vinken K., Lenaerts S. (2011), Photocatalytic degradation of ethylene: An FTIR in situ study
 340 under atmospheric conditions, *Appl. Catal. B Environ.* 105 : 111–116.

341 -Iliev V., Tomova D., Bilyarska L., Tyuliev G. (2007), Influence of the size of gold
 342 nanoparticles deposited on TiO₂ upon the photocatalytic destruction of oxalic acid, *J. Mol.*
 343 *Catal. Chem.* 263 : 32–38.

344 -Jacobson M.Z. (2002), Atmospheric pollution: history, science, and regulation, Cambridge
 345 University Press.

346 -Jia Z. (2013), Elaboration des matériaux composites nanostructurés Ag, Au/TiO₂ pour la
 347 dépollution des effluents gazeux avec une activation par plasma, Université Paris 13.

348 -Joris S. J., Amberg C. H. (1971), J. Phys. Chem. , 75 : 316

349 -Kamat P.V. (2002), Photophysical, photochemical and photocatalytic aspects of metal
 350 nanoparticles, J. Phys. Chem. B. 106 : 7729–7744.

351 -Kibby C.L., Lande S.S., Hall W.K. (1972), Tracer studies of acid-catalyzed reactions. XI.
 352 Stereoselectivity in alcohol dehydration over hydroxyapatite and alumina catalysts, J. Am.
 353 Chem. Soc. 94 : 214–220.

354 -Krestou A., Xenidis A., Panias D. (2004), Mechanism of aqueous uranium (VI) uptake by
 355 hydroxyapatite, Miner. Eng. 17 : 373–381.

356 -Li P., Nakanishi K., Kokubo T., de Groot K. (1993), Induction and morphology of
 357 hydroxyapatite, precipitated from metastable simulated body fluids on sol-gel prepared silica,
 358 Biomaterials. 14 : 963–968.

359 -Lopez L., Daoud W.A., Dutta D., Panther B.C., Turney T.W. (2013), Effect of substrate on
 360 surface morphology and photocatalysis of large-scale TiO₂ films, Appl. Surf. Sci. 265 : 162–
 361 168.

362 -Ma Q.Y., Traina S.J., Logan T.J., Ryan J.A. (1994), Effects of aqueous Al, Cd, Cu, Fe (II),
 363 Ni, and Zn on Pb immobilization by hydroxyapatite, Environ. Sci. Technol. 28 : 1219–1228.

364 -Matsumura Y., Kanai H., Moffat J.B (1997), Catalytic oxidation of carbon monoxide over
 365 stoichiometric and non-stoichiometric hydroxyapatites, J. Chem. Soc. Faraday Trans. 93 :
 366 4383–4387.

367 -Matsumura Y., Moffat J.B. (1994), Partial Oxidation of Methane to Carbon-Monoxide and
 368 Hydrogen with Molecular-Oxygen and Nitrous-Oxide over Hydroxyapatite Catalysts, J. Catal.
 369 148 : 323–333.

370 -Matsumura Y., Moffat J.B. (1996), Methanol adsorption and dehydrogenation over
 371 stoichiometric and non-stoichiometric hydroxyapatite catalysts, J Chem Soc Faraday Trans.
 372 92 : 1981–1984.

373 -Mitsionis A., Vaimakis T., Trapalis C., Todorova N., Bahnemann D., Dillert R. (2011),
 374 Hydroxyapatite/titanium dioxide nanocomposites for controlled photocatalytic NO oxidation,
 375 Appl. Catal. B Environ. 106 : 398–404.

376 -Monma H. (1982), Catalytic behavior of calcium phosphates for decompositions of 2-
 377 propanol and ethanol, J. Catal. 75 : 200–203.

378 -Nasr-Esfahani M., Fekri S. (2012), Alumina/TiO₂/hydroxyapatite interface nanostructure
 379 composite filters as efficient photocatalysts for the purification of air, React. Kinet. Mech.
 380 Catal. 107 : 89–103.

381 -Nathanael A. J., Mangalaraj D., Chen P.C., Ponpandian N. (2010), Mechanical and
 382 photocatalytic properties of hydroxyapatite/titania nanocomposites prepared by combined
 383 high gravity and hydrothermal process, Compos. Sci. Technol. 70 : 419–426.

384 -Nishikawa H., Omamiuda K. (2002), Photocatalytic activity of hydroxyapatite for methyl
 385 mercaptane, J. Mol. Catal. Chem. 179 : 193–200.

386 -Nonami T. (2004), Apatite-Coated Titanium Dioxide Photocatalyst for Air Purification,
 387 Catal. Today. 96 : 113–118.

388 -Qian G., Li M., Wang F., Liu X. (2014), Removal of Fe³⁺ from Aqueous Solution by
 389 Natural Apatite, J. Surf. Eng. Mater. Adv. Technol.

390 -Smeulders D. E., Wilson M.A., Armstrong L. (2001), Insoluble organic compounds in the
 391 Bayer process, Ind. Eng. Chem. Res. 40 : 2243–2251

392 -Smith K. (1989), Modern Powder Diffraction”; in Review in Mineralogy, Edited by D. L.
 393 Bish and J. E. Post. Mineralogical Society of America, Washington, DC, 20 : 183.

394 -Tanaka H., Tsuda E., Nishikawa H., Fuji M. (2012), FTIR studies of adsorption and
 395 photocatalytic decomposition under UV irradiation of dimethyl sulfide on calcium
 396 hydroxyapatite, Adv. Powder Technol. 23 : 115–119.

397 -Tieng S, Kanaev A and Chhor K. (2011) New homogeneously doped Fe(III)-TiO₂
 398 photocatalyst for gaseous pollutant degradation, J Appl Catal A 399: 191-197.

399 -Tieng S, Jia Z., Diaz-Gomez Trevino A. P., Eloy P., Giagneaux E. M., Chhor K., Kanaev A.
 400 (2019) Major non-volatile intermediate products of photo-catalytic decomposition of
 401 ethylene, Journal of Catalysis 374: 328-334.

402 -Tsukada M., Wakamura M., Yoshida N., Watanabe T. (2011), Band gap and photocatalytic
 403 properties of Ti-substituted hydroxyapatite: comparison with anatase-TiO₂, J. Mol. Catal.
 404 Chem. 338 : 18–23.

405

FIGURES

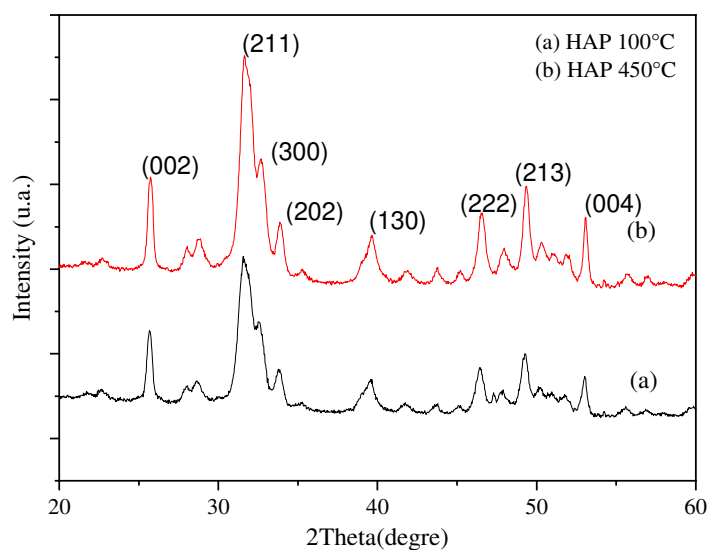


Fig. 1: Heat-treated hydroxyapatite diffraction patterns at 100°C (a) and 450°C (b).

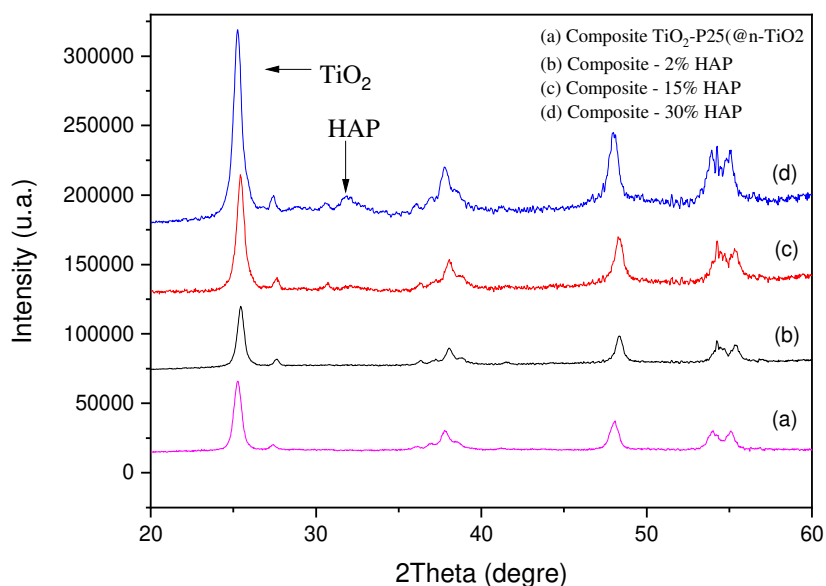


Fig. 2: X-ray diffractograms of samples of TiO_2 -P25 @ n- TiO_2 / HAP composite treated with different mass compositions of hydroxyapatite (a) 0% (b) 2% (c) 15% and (d) 30%.

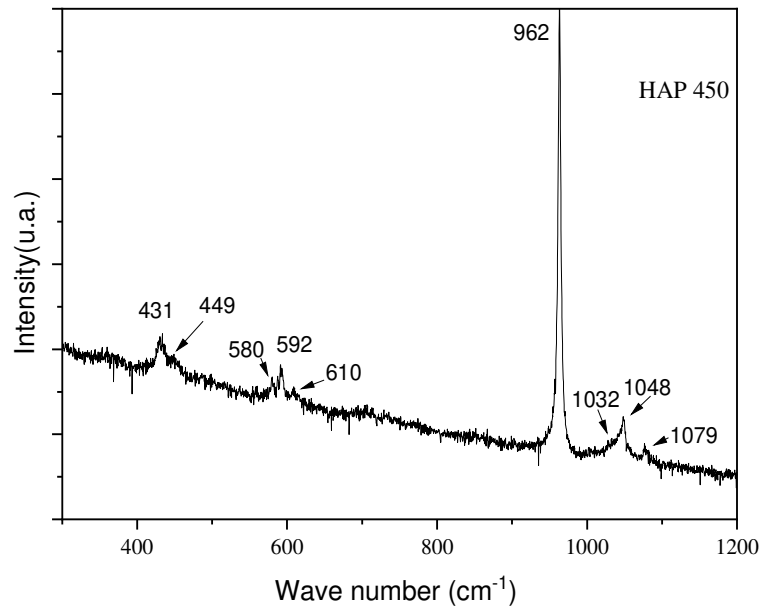


Fig. 3: Raman spectrum of hydroxyapatite treated at 450 ° C recorded with excitatory

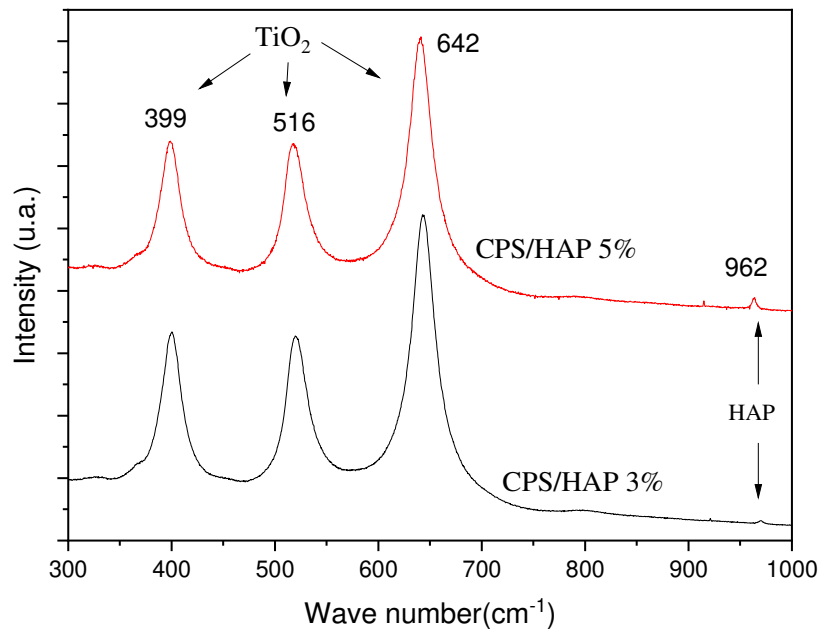


Fig. 4: Raman spectra of two CPS / PAH samples loaded with 3 and 5% PAH and treated at 450 ° C for 4 h.

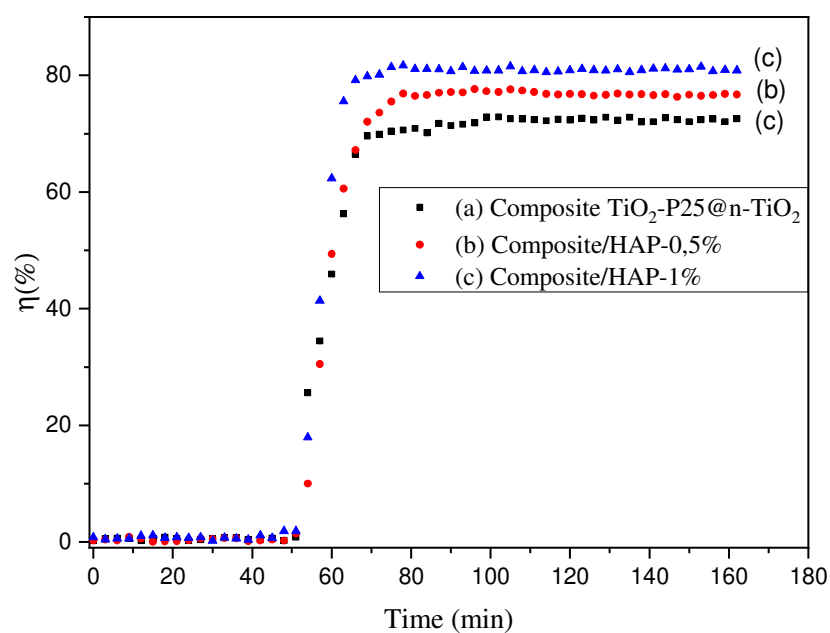


Fig. 5: Evolution of the photodegradation of ethylene by CPS / HAP-0.5 and CPS / HAP-1 as a function of the irradiation time. The conversion rate of ethylene by the untreated composite is given for comparison. ($\lambda = 360 \text{ nm}$, ethylene 150 ppm, flow rate $10 \text{ mL} \cdot \text{min}^{-1}$).

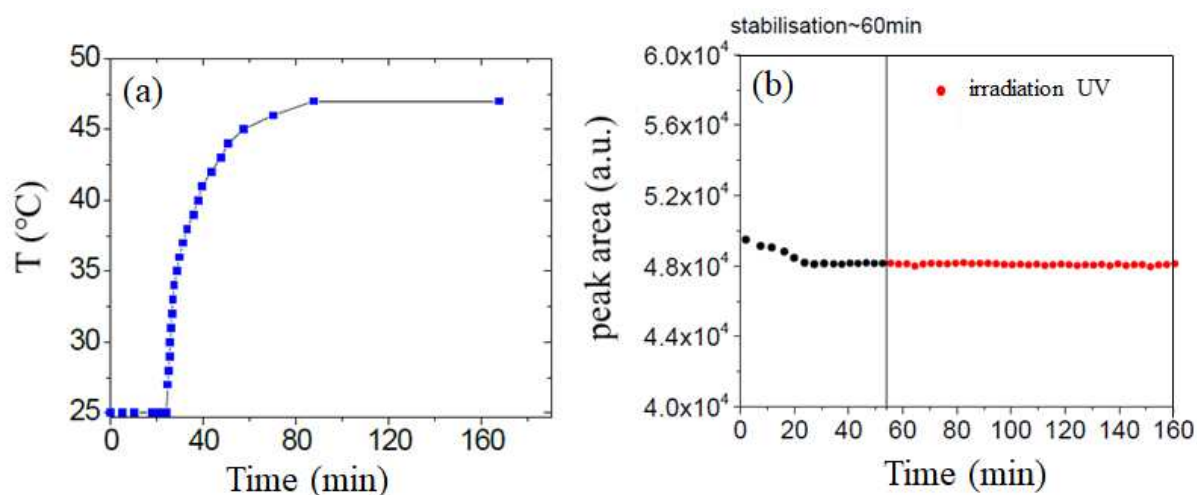


Fig. 6: Temperature evolution during photocatalytic tests (a) and Ethylene concentration evolution under UV irradiation without photocatalysts (b).

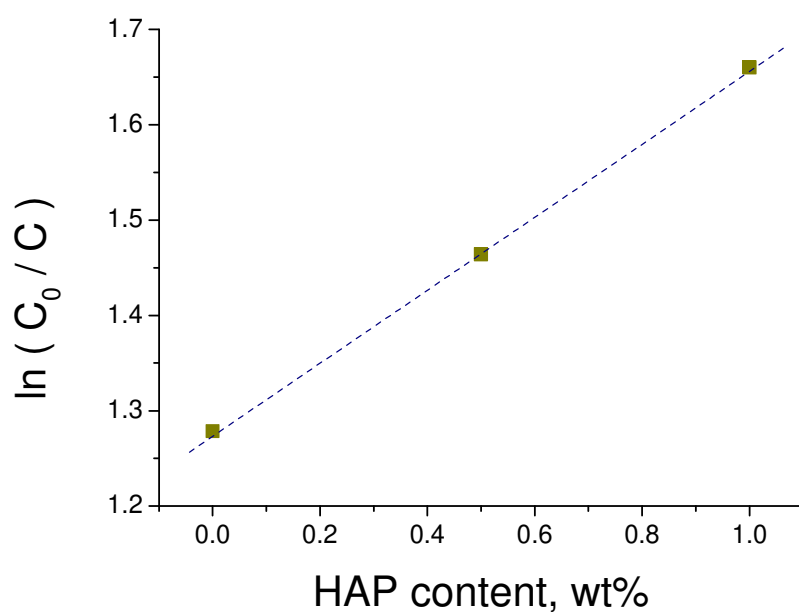


Fig. 7: Photocatalytic activity as a function of HAP doping.

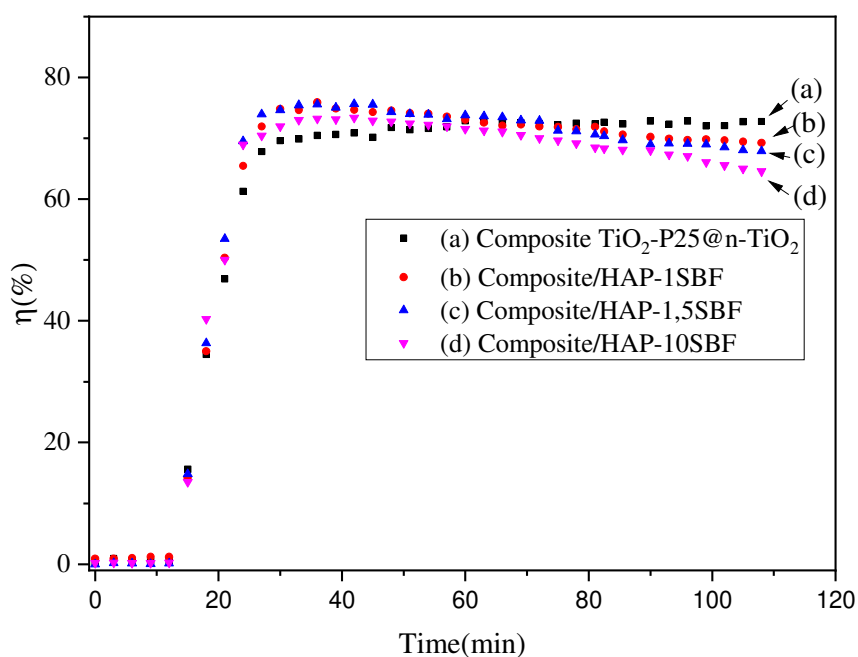
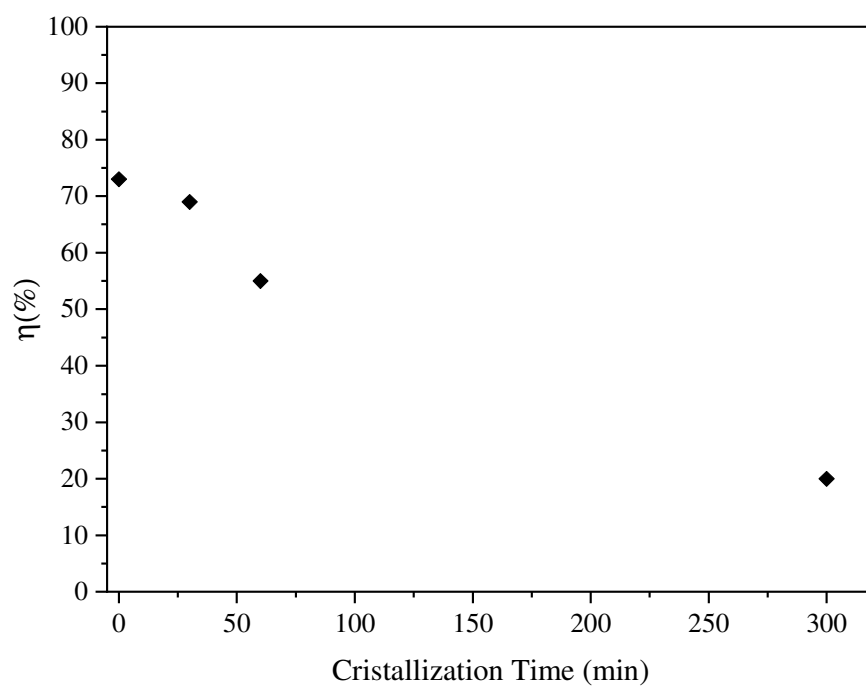


Fig. 8:

Evolution of the photodegradation of ethylene by different CPS / HAP-SBF as a function of the irradiation time. The conversion rate of ethylene by the untreated composite is given for comparison. ($\lambda = 360 \text{ nm}$, ethylene 150 ppm, flow rate 10 mL.min^{-1}).



440
 441 *Fig. 9: Photodegradation of ethylene by CPS / HAP-LSBF as a function of the crystallization*
 442 *time. ($\lambda = 360 \text{ nm}$, ethylene 150 ppm, flow rate $10 \text{ mL} \cdot \text{min}^{-1}$).*